Ecological Modelling 451 (2021) 109578

Contents lists available at ScienceDirect

Ecological Modelling

journal homepage: www.elsevier.com/locate/ecolmodel

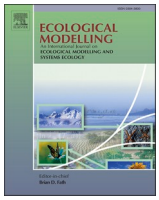

Global assessment of marine phytoplankton primary production: Integrating machine learning and environmental accounting models

F. Mattei [a,c,d,*], E. Buonocore [b,c], P.P. Franzese [b,c], M. Scardi [a,c]

[a] Department of Biology, University of Rome "Tor Vergata", Via della Ricerca Scientifica, 00133 Rome, Italy
[b] UNESCO Chair in "Environment, Resources and Sustainable Development", Department of Science and Technology, Parthenope University of Naples, Via F. Petrarca n. 80, (80123) Naples, Italy
[c] CoNISMa, Piazzale Flaminio, 9, 00196, Rome, Italy
[d] Ph.D. Program in Evolutionary Biology and Ecology, Department of Biology, University of Rome Tor Vergata, 00133 Rome, Italy

ARTICLE INFO

Keywords:
Phytoplankton primary production
Systems ecology
Artificial neural networks
Machine learning
Emergy accounting

ABSTRACT

The emergy accounting method has been widely applied to terrestrial and marine ecosystems although there is a lack of emergy studies focusing on phytoplankton primary production. Phytoplankton production is a pivotal process since it is intimately coupled with oceanic food webs, energy fluxes, carbon cycle, and Earth's climate. In this study, we proposed a new methodology to perform a biophysical assessment of the global phytoplankton primary production combining Machine Learning (ML) techniques and an emergy-based accounting model. Firstly, we produced global phytoplankton production estimates using an Artificial Neural Network (ANN) model. Secondly, we assessed the main energy inputs supporting the global phytoplankton production. Finally, we converted these inputs into emergy units and analysed the results from an ecological perspective. Among the energy flows, tides showed the highest maximum emergy contribution to global phytoplankton production highlighting the importance of thise flow in the complex dynamics of marine ecosystems. In addition, an emergy/production ratio was calculated showing different global patterns in terms of emergy convergence into the primary production process. We believe that the proposed emergy-based assessment of phytoplankton production could be extremely valuable to improve our understanding of this key biological process at global scale adopting a systems perspective. This model can also provide a useful benchmark for future assessments of marine ecosystem services at global scale.

1. Introduction

Ecosystems are open, far from thermodynamic equilibrium, and hierarchically self-organized systems characterized by complex networks and emergent properties (Buonocore et al., 2019; Jørgensen et al., 2011; Jørgensen and Fath, 2004).

Several functions have been identified as principles able to explore ecosystems complexity and development. These functions are known as Goal Functions (GFs) and can be divided into three macro-categories: the biotic, the network, and the thermodynamic GFs (Jørgensen and Mejer, 1979; Vihervaara et al., 2019). Among the thermodynamic GFs, emergy was introduced by H.T. Odum to unfold the role of matter and energy flows in supporting both natural and human-dominated ecosystems (Odum, 1996, 1988).

The Emergy accounting method has been widely applied to explore terrestrial and marine ecosystems (Franzese et al., 2020, 2019, 2014; Pulselli et al., 2011). Recent studies provided an assessment of the biophysical value of natural capital and ecosystem services in marine ecosystems by using the emergy accounting method. Vassallo et al. (2017) developed a biophysical and trophodynamic model based on emergy accounting to assess the value of natural capital in marine protected areas (MPAs). Franzese et al. (2017), Picone et al. (2017), and Paoli et al. (2018) applied the model described in Vassallo et al. (2017) for assessing the biophysical and economic value of natural capital in selected Mediterranean MPAs. Berrios et al. (2017) used emergy accounting to assess natural capital and ecosystem services of benthic marine ecosystems in Chile, also exploring their contributions to the well-being of regional economy. Berrios et al. (2018) evaluated the ecosystem health of three benthic marine networks in northern Chile by using energy systems theory and emergy accounting. Buonocore et al.

* Corresponding author.
E-mail address: francesco.mattei90@yahoo.it (F. Mattei).

https://doi.org/10.1016/j.ecolmodel.2021.109578
Received 12 November 2020; Received in revised form 19 March 2021; Accepted 21 April 2021
Available online 3 May 2021

(2020a, 2020b) used the emergy method to assess the value of marine natural capital stocks in southern Italy. Yang et al. (2019) implemented an emergy-based assessment for coastal and marine ecosystem services in China.

While many emergy studies have been applied to explore benthic marine ecosystems, there is a lack of emergy studies focusing on marine primary production in the water column at both local and global scales. In the context of marine ecosystems, phytoplankton primary production is a crucial biological process since it accounts for about 94% and 50% of marine and global autotrophic production (Duarte and Cebrián, 1996). Accordingly, phytoplankton production represents the bulk of energy for structuring marine food webs, allowing the generation of natural capital stocks and the delivery of provisioning, regulating, and cultural ecosystem services (Blythe et al., 2020; Buonocore et al., 2020a; Chakraborty et al., 2020). Furthermore, phytoplankton production exerts a regulating effect on Earth's climate through a net uptake of CO_2 from the atmosphere with a share of the fixed carbon removed from the fast carbon cycle through sinking of organic matter (Longhurst and Glen Harrison, 1989).

For these reasons, phytoplankton production is a pivotal component of marine ecosystems functioning and enhancing its understanding is a central issue in modern oceanography.

The study of marine phytoplankton production on a global scale requires to be supported by ecological models. This support maximizes theinformation derived from in situ measurements which are expensive and time-consuming. Several models were developed to estimate primary production from ocean color and some of them were compared in published studies (Carr et al., 2006; Friedrichs et al., 2009; Lee et al., 2015; Saba et al., 2011). Among the available phytoplankton production estimators, the one developed by Scardi (2001) is based on a Machine Learning (ML) technique, i.e. Artificial Neural Network (ANN).

The strengths of the ML approaches rely on the ability to handle complex and non-linear relationships, which are ubiquitous in natural systems (Catucci and Scardi, 2020; Franceschini et al., 2019; Lek et al., 1996; Mattei and Scardi, 2020; Olden et al., 2008). Moreover, they can exploit a wide range of predictive variables, since no a priori explicit mathematical formulation of the link between predictive variables and the output is needed. The latter feature is extremely valuable when remotely-sensed information is taken into account.

Since phytoplankton primary production is a central process in the marine ecosystem functioning, several research areas could benefit from a deepening in the understanding of its dynamics. From a climate perspective, a global assessment of phytoplankton production could improve the comprehension of climate change effects on this process and to the ones related to it, such as the global carbon cycle (Blanchard et al., 2012; Barange et al., 2014; Maureaud et al., 2017; Behrenfeld et al., 2006; Boyce et al., 2010). Moreover, several marine ecosystem services and functions are related to phytoplankton autotrophic production (Buonocore et al., 2019; Costanza et al., 1997; Melaku Canu et al., 2015; Richardson and Schoeman, 2004). Accordingly, the management of the marine system and its resources is deeply linked with the characteristics of this biological process (Nixon, 1992; Conti and Scardi, 2010; Russo et al., 2019).

In this work, we developed and applied a novel methodology to perform a biophysical assessment of the global phytoplankton primary production combining ML techniques and an emergy-based environmental accounting model.

2. Materials and methods

The integrated modeling approach implemented in this study could be divided in three main steps. Firstly, we estimated the global phytoplankton production using an ANN model, which requires only predictive variables that can be either retrieved from remote sensing platforms or derived from them. The latter feature allows the model user to freely retrieve the needed information from online repositories. Secondly, we gathered all the information about the main energy inputs converging to the marine ecosystem and influencing the phytoplankton production. Matter inputs to the primary production can be mainly considered as quantities continuously recycling into the system on a global scale. For this reason, we assumed that matter inputs do not carry any emergy value and were not considered for the emergy analysis in this work. Finally, we converted the energy inputs into emergy units and explored our results using data analysis and visualization tools.

The methodology was applied on data referred to the year 2018 since it was the most recent year for which all the needed data were available. The main steps of our approach are described in the following paragraphs.

2.1. Phytoplankton primary production model

We used an ANN model (Scardi, 2001) to estimate integrated phytoplankton primary production on a global scale. The ANN was trained with a classic version of the error back-propagation algorithm (Rumelhart et al., 1986). The software used to train the ANN was developed in Fortran 90. The Fortran program and a python script to estimate the phytoplankton production are available upon request.

The predictive variables included the day of the year and the geographic coordinates of the selected area. The coordinates were extracted from a 4320 × 8640 matrix (latitude x longitude) with a resolution of 0.041 × 0.041°. This resolution was selected for consistency with the MODIS-aqua data. The day of the year was set as the 15th day of each month to provide a mean monthly estimate. The day of the year and the longitude were passed as input after a trigonometric transformation which produced two derived variables, while the latitude was not transformed (Mattei et al., 2018; Scardi, 2001). The model also needed the surface irradiance (Frouin et al., 2012; Frouin and Pinker, 1995), sea surface temperature (Werdell et al., 2013), and surface chlorophyll *a* concentration (Hu et al., 2012; Morel and Maritorena, 2001; O'Reilly et al., 1998; Werdell and Bailey, 2005). These predictors can be downloaded from the MODIS-Aqua repository at the following link https://oceandata.sci.gsfc.nasa.gov/MODIS-Aqua/Mapped/Monthly/4km/. These environmental variables are available with a resolution of 0.041 × 0.041° (4320 × 8640 latitude x longitude grids). The last three predictive variables were computed using models or mathematical equations. The first was the mixed layer depth, which could be estimated using several models, e.g. Monterey and Levitus (Levitus et al., 1994; Levitus and Boyer, 1994). The second one was the daylength, which we computed as function of the day of the year and latitude.

The last one was the P^B_{opt} which is a physiological variable computed as function of the sea surface temperature (Behrenfeld and Falkowski, 1997).

A list of the ANN model inputs and output is shown in Table 1.

After retrieving the predictive variables, we used the ANN model to estimate the mean phytoplankton production on a global scale for each month of the year 2018. We kept the 4 km resolution of the MODIS-Aqua data, thus producing a 4320 × 8640 grid (0.041 latitude x 0.041 longitude degrees) ASCII file for each month containing the production appraisals. Subsequently, we used these files to generate global production maps. Figure 1 shows the global production map generated for January 2018. The maps generated for all the months of the year are available in the online supplementary materials.

The missing values shown as black pixels in Fig. 1 represent the areas for which the predictive variables were not available. The lack of information was mainly due to the cloud coverage of the ocean which impeded the measurement of surface chlorophyll *a* from remote sensing platforms. This phenomenon was not homogeneous neither spatially nor temporally. In fact, the main affected areas were those at higher latitude with different patterns throughout the year (see supplementary materials and Figs. 5-8).

Table 1
Artificial neural network inputs and output.

ANN inputs	Units	Resolution	Source	Algorithm
Surface chlorophyll *a*	mg m^{-3}	0.041 × 0.041 degrees (lat x lon)	MODIS-aqua	Hu et al. (2012)
Surface irradiance	E m^{-2} day^{-1}	0.041 × 0.041 degrees (lat x lon)	MODIS-aqua	Frouin and Pinker, 1995
S ea surface temperature	°C	0.041 × 0.041 degrees (lat x lon)	MODIS-aqua	Werdell et al., 2013
Mixed layer depth	M	0.25 × 0.25 degrees (lat x lon)	Levitus MLD	Levitus et al. (1994)
P^B_{opt}	mg C (mg chl)$^{-1}$ h^{-1}	0.041 × 0.041 degrees (lat x lon)	Behrenfeld and Falkowski (1997)	Function of sea surface temperature
Day length	h	/	/	Function of latitude and day of the year
Latitude	degrees	/	/	/
sin(longitude)	–	/	Scardi, 2001	Trigonometric transformation
cos(longitude)	–	/	Scardi, 2001	Trigonometric transformation
sin(date)	–	/	Scardi, 2001	Trigonometric transformation
cos(date)	–	/	Scardi, 2001	Trigonometric transformation
ANN output	Units			
Integrated Phytoplankton Production	mg C m^{-2} day^{-1}	0.041 × 0.041 degrees (lat x lon)	Scardi, 2001	ANN model

2.2. Energy inputs

We relied on both the ecological knowledge of the phytoplankton production process (Reynolds, 2006) and the current literature on emergy accounting (Brown and Ulgiati, 2016a; Campbell and Tilley, 2016; Lee et al., 2019) to identify and assess the main energy inputs supporting phytoplankton primary production at global scale (Fig. 2). The energy inputs can be divided in primary and secondary sources. The primary renewable energy inputs, also known as the global tripartite, comprise the solar, tidal, and geothermal exergy (Brown et al., 2016). The secondary renewable energy sources are generated by the interactions of the primary ones.

The first primary renewable input taken into account was the solar energy. We converted the same Photosynthetically Active Radiation (PAR) data used as input for the ANN model into total solar radiation (total radiation = 2.32 PAR). This variable showed the higher resolution among the gathered data and was stored in a 4320 × 8640 grid (0.041 latitude x 0.041 longitude degrees).

The unit of measure was converted from E m^{-2} day^{-1} to J m^{-2} day^{-1} to evaluate the energy contribution to the system. This was not a straightforward operation since the former measures energy quanta while the latter refers to an energy flux. We used the relationship found by Britton and Dodd (1976) (1 μE m^{-2} s^{-1} corresponds to 0.219 W m^{-2}) to convert μE m^{-2} s^{-1} to W m^{-2}. Then, we obtained J s^{-1} since by definition 1 $W = 1$ J s^{-1} and the J m^{-2} day^{-1} multiplying by the second in a day. The solar energy input was calculated according to the following equation:

$$E_{sunlight} = 0.219\ E\ T \quad (1)$$

Where $E_{sunlight}$ is the solar energy expressed as J m^{-2} day^{-1}, while E is the solar energy expressed as μE m^{-2} s^{-1} and T are the seconds in a day.

Moreover, the tidal energy, which plays an important role in the water column mixing and ocean circulation (Blauw et al., 2012; Cadier et al., 2017; Jorge and Beusekom, 1995), was assessed on the base of information retrieved from the Swedish National Data Service (https://snd.gu.se/en/catalog/study/ecds0243/001). The dimensionality of the data grid was 2880 × 5760 (0.062 latitude x 0.062 longitude degrees). We computed the energy contribution of tides using the following formula:

$$E_{tides} = \frac{1}{2}\ \frac{N_t}{365}\ h^2\ \rho_w\ g \quad (2)$$

Where N_t is the annual number of tidal cycles, h^2 is the annual average cycle amplitude (m), ρ_w is the sea water density (1030 kg m^{-3}) and g is the acceleration of gravity (9.8 m s^{-2}).

Finally, we accounted for the surface heat flow that is a crucial process in the Earth's energy dynamics (Beardsmore et al., 2001) since it represents one of the interfaces between Earth's solid interior, hydrosphere, cryosphere, and atmosphere (Fahnestock et al., 2001; Mashayek et al., 2013; Scott et al., 2001). The global surface heat flow map produced by Davies (2013) was used to assess the heat flow energy contribution. The map was available as a 90 × 180 (1 latitude x 1

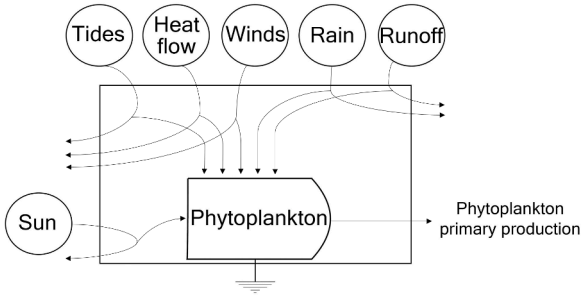

Fig. 2. Systems diagram showing energy inputs supporting phytoplankton primary production.

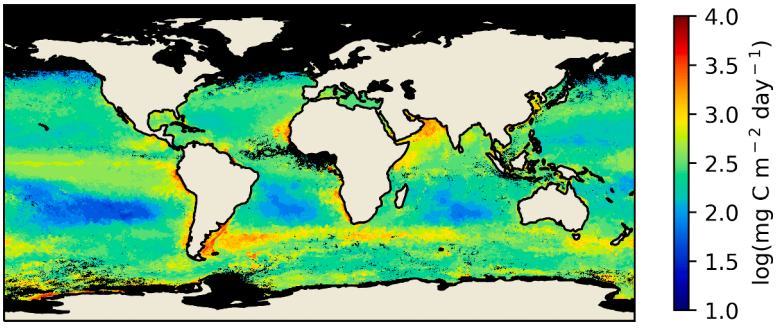

Fig. 1. Integrated phytoplankton primary production map of January 2018 (log(mg C m^{-2} day^{-1})).

longitude degree) grid and the heat flow data were stored as mW m^{-2}. We converted the values into J m^2 day^{-1} to assess the heat flow daily energy. Finally, to assess the exergy contribution we used an average Carnot efficiency of 69% (Lee et al., 2019).

Regarding the secondary energy inputs, the wind stress on the ocean surface was firstly considered. This stress influences the water column physical dynamics, which in turn deeply affect phytoplanktonic organisms (Jorge and Beusekom, 1995; Manwell et al., 2010). We retrieved the wind speed from the ERA5 monthly averaged data (Hersbach et al., 2019), which are stored in the Copernicus Climate Data Store (CDS). The wind energy contribution to the marine systems has been calculated following the procedure developed by Brown and Ulgiati (2016a). We computed the geostrophic wind velocity using the 10 m wind speed according to the following formula (3):

$$V = V_{ref}\left(\frac{H}{H_{ref}}\right)^{\alpha} \quad (3)$$

Where V is the geostrophic wind velocity, V_{ref} is the reference velocity (wind speed at 10 m), H is the height for the geostrophic wind (1000 m), H_{ref} is the reference height (10 m) and α is the surface roughness exponent (0.1) (Manwell et al., 2010). Subsequently, the wind energy contribution was assessed according to the following formula (4):

$$E_{wind} = \frac{1}{2}\ \rho_a\ KGN\ V^3\ A\ T \quad (4)$$

Where ρ_a (1.229 kg m^{-3}) is the air density at sea level, *KNG* is a geostrophic drag coefficient (1.26 10^{-3}) (Garratt, 1994), A is an area of 1 m^2, and T are the seconds in a day.

The chemical potential of rainfall over the ocean (Brown and Ulgiati, 2016b; Lee et al., 2019) was assessed on the base of precipitation data retrieved from the ERA5 monthly averaged data, stored as m day^{-1} and in a 720 × 1440 grid (0.25 latitude x 0.25 longitude degrees). We computed the rain energy contribution according to the following equation:

$$E_{rain} = r\ \rho_w\ G \quad (5)$$

Where r is the rainfall (m day^{-1}), ρ_w is the sea water density (1030 kg m^{-3} = 1030 10^3 g) and G is the Gibbs constant (4.72 J g^{-1}) (Lee et al., 2019).

Based on the ERA5 monthly averaged data, we also assessed the terrestrial runoff that is an important nutrient input in coastal areas where it is accountable due to their higher production magnitude compared to open ocean. Data were stored in a 720 × 1440 (0.25 latitude x 0.25 longitude degrees) grid and expressed in m day^{-1}.

The chemical potential of runoff was computed through the following equation:

$$E_{runoff} = R\ \rho_w\ G \quad (6)$$

Where R is the runoff expressed as m day^{-1}, ρ_w is the water density (10^6 g m^{-3}) and G is the Gibbs constant (4.72 J g^{-1}).

2.3. Emergy accounting

Emergy measures the cumulative environmental support to a process (Odum, 1996, 1988). Emergy accounting aims at evaluating the environmental performance of a system on the global scale of the biosphere, taking into account free environmental inputs driving the functioning of natural systems (e.g., solar radiation, wind, rain, and geothermal flow) and human-driven flows driving socioeconomic systems (Brown and Ulgiati, 2016c, 2016a; Franzese et al., 2014, 2009). According to this method, inputs are accounted for in terms of their solar emergy, defined as the total amount of solar available energy (exergy) directly or indirectly required to make a given product or support a given flow, and measured in sej (solar emergy joules). The solar emergy required to generate one unit of product or service is referred to as Unit Emergy Value (UEV, sej J^{-1}, sej g^{-1}). Mass and energy inputs to the investigated system are converted into emergy units by using appropriate UEVs, and then summed to calculate the total emergy support.

After the evaluation of the main energy inputs converging to the marine ecosystem and driving the phytoplankton production, we converted them into emergy inputs (sej m^{-2} day^{-1}) by using specific Unit Emergy Values (UEVs, sej J^{-1}, sej g^{-1}) (table 2). The UEVs were updated to the last emergy baseline (1.20 10^{25} sej $year^{-1}$) computed by Brown et al. (2016).

Once the emergy inputs were assessed, we summed them to evaluate the total emergy supporting phytoplankton production for each month of the 2018. The total emergy was calculated following the emergy algebra rules according to the following formula proposed by Brown and Ulgiati (2016):

$$Em_{tot} = max\left(\left(Em_{sun} + Em_{tides} + Em_{heat\ flow}\right),\ Em_{wind},\ Em_{rain},\ Em_{runoff}\right) \quad (7)$$

This method compares the sum of the global tripartite with the largest of secondary and tertiary sources taking the larger of these two values as the emergy input. Following this procedure, we produced 12 grids, with a spatial resolution of 4320 × 8640 (0.041 latitude x 0.041 longitude degrees) one for each month of 2018, in which we computed the emergy value of phytoplankton production for each pixel. Subsequently, we mapped these grids and we computed an emergy/production ratio in order to highlight different global patterns in the emergy conversion into primary production (Fig. 5-8 and supplementary materials). As pointed out in Section 2.1, missing values in the grids and on the maps refer to missing value of the predictive variables used to estimate the primary production.

Finally, to analyze the temporal variability of the emergy/production ratio, we computed its variance for the 2018. The variance was computed using the values of each month for the same pixel. In order to avoid biases, we calculated the variance only for the pixels that showed at least 6 values out of 12 and less than 3 missing values in a row (Fig. 9).

3. Results and discussion

3.1. Energy inputs magnitude, variability and hierarchy

Once assessed the contribution of the energy inputs to the marine system, we analysed their magnitude and hierarchy (Fig. 3). Among the renewable energy input supporting phytoplankton primary production solar exergy had the larger maximum, minimum and average values for the year 2018 (Table 3).

This is not surprising since this component of the global tripartite is the main available source of energy for the biosphere and it allows the generation and the maintenance of natural systems far from thermodynamic equilibrium, e.g. ecosystems. In fact, the solar energy exploitation by photosynthetic organisms, which convert this free energy flux into chemical bonds, fuels the bulk of natural systems. The global interannual variability of solar energy was not as pronounced as the one associated with other inputs. In fact, it was the only exergy source which showed a maximum and an average value of the same order of magnitude, i.e. 10^7 J m^{-2} day^{-1} (Fig. 3).

Table 2
UEVs used in this study and respective references.

Input	UEV (sej J^{-1}; sej g^{-1})	Reference
Sunlight	1.00	By definition
Tides	3.09 10^4	(Brown and Ulgiati, 2016a)
Heat flow	4.9 10^3	(Brown and Ulgiati, 2016a)
Wind	5.2 10^2	Lee et al. 2019
Rainfall	4.9 10^3	(Brown and Ulgiati, 2016a)
Runoff	2.09 10^4	Lee et al. 2019

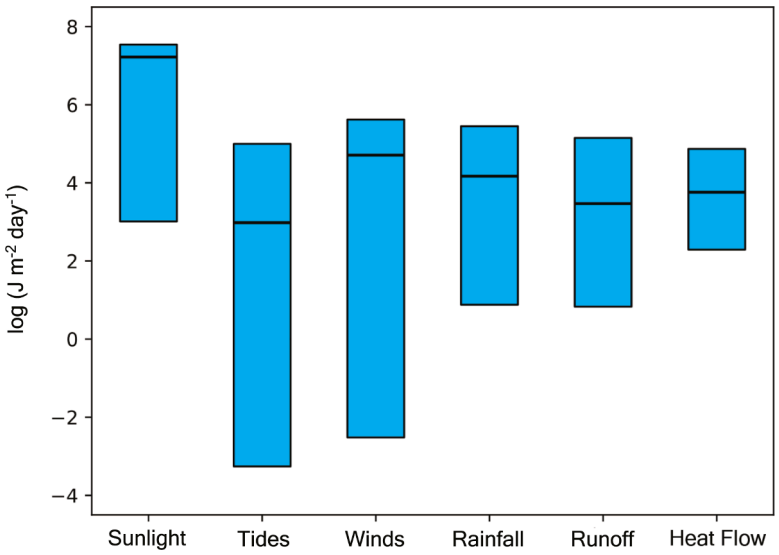

Fig. 3. Daily energy inputs in 2018. The bar chart shows the range and the average daily energy contribution for each input in the considered year.

Table 3
Global daily energy inputs. The table shows the maximum, minimum and average values for the energy inputs supporting global phytoplankton production.

Input	Max (J m^{-2} day^{-1})	Min (J m^{-2} day^{-1})	Avg (J m^{-2} day^{-1})
Sunlight	3.49 10^7	1.02 10^3	1.67 10^7
Tides	9.99 10^4	5.40 10^{-4}	9.56 10^2
Wind	4.21 10^5	3 10^{-3}	5.12 10^4
Rainfall	2.82 10^5	7.51	1.49 10^4
Runoff	1.41 10^5	6.83	2.98 10^3
Heat flow	7.37 10^4	1.94 10^2	5.81 10^3

Tidal energy was the second member of the global tripartite that showed a large free energy contribution. Its maximum value was the closest to the solar one but its global variability showed different features. In fact, maximum and minimum tidal contribution where the most distant from each other showing a magnitude of 10^4 and 10^{-4} respectively (Table 3). This feature reflects the differences of tidal amplitude in distinct areas, especially between open ocean and costal zones. From an ecological perspective, tides deeply influence the ocean physical dynamics which in turn affect the living organism especially the planktonic ones. In fact, tides generate tidal currents which in turn influence the dynamic of the water column. Moreover, tidal mixing phenomena generates upwelling of nutrients from deeper waters to the euphotic zone thus affecting phytoplankton composition and production ((Jorge and Beusekom, 1995)Blauw et al., 2012; Cadier et al., 2017).

The contribution of geothermal flow was lower than the other two primary renewable resources with an average global contribution of 5.81 10^3 J m^{-2} day^{-1} (Table 3). On the other hand, it showed the smaller distance between maximum and minimum among all the energy sources taken into account, i.e. only two orders of magnitude. The role of the heat flow on large scale circulation and tracer distribution was highlighted by several studies with particular emphasis for the deep ocean circulation (Beardsmore et al., 2001; Mashayek et al., 2013; Scott et al., 2001). Accordingly, global circulation patterns and nutrients upwelling phenomena, which deeply influence global phytoplankton production, are related to this energy source.

The wind energy input showed characteristics similar to tidal energy. Its maximum value was several orders of magnitude larger than its minimum (Fig. 3). Conversely, the maximum value of wind energy contribution to the marine system was lower than the tidal one while its global average was larger. From a global perspective, surface circulation is deeply influenced by winds net input of kinetic energy into the oceans. Furthermore, the winds-ocean interaction supports the formation of waves and deep stable stratification both of which affect living organisms within the water column (Jorge and Beusekom, 1995; Manwell et al., 2010; Zhai, 2013).

The rainfall and runoff contribution to the marine system has been taken into account as chemical potential, which can be defined as the tendency of a substance to change (Job and Herrmann, 2006). The contribution of the precipitation resulted larger from a maximum, minimum and average perspective compared to runoff (Fig. 3). This difference was particularly evident when the average was taken into account. In fact, while the difference does not seem high for the maximum and minimum values, the rainfall average contribution was an order of magnitude larger than the runoff one (Table 3). Rainfall influences several aspects of the ocean surface such as temperature and salinity. These physical characteristics in turn affect both sea water density and interactions with the atmosphere determining stratification phenomena and gas solubility (Doney, 1995; Schlössel et al., 1997).

Although the runoff maximum contribution was lower than the other secondary energy inputs, it was of the same magnitude order (10^5). On the other hand, runoff showed the lowest global average value (Fig. 3) since its effect is limited to coastal areas where its contribution to the marine system and primary production is not negligible. In fact, it provides new nutrients from land ecosystems thus boosting phytoplankton production, which is frequently nutrient limited (Chase et al., 2007; Spatharis et al., 2008).

3.2. *Emergy inputs magnitude, variability and hierarchy*

Table 4 shows the emergy value of the energy inputs supporting global phytoplankton production. The emergy values are compared in Fig. 4.

Table 4
Global daily emergy 2018. The table shows the maximum, minimum and average daily emergy values supporting global phytoplankton production.

Input	Max (sej m^{-2} day^{-1})	Min (sej m^{-2} day^{-1})	Avg (sej m^{-2} day^{-1})
Tides	3.09 10^9	16.7	2.95 10^7
Runoff	2.94 10^9	1.43 10^5	6.23 10^7
Rainfall	1.38 10^9	3.68 10^4	7.29 10^7
Heat flow	3.61 10^8	9.49 10^5	2.85 10^7
Wind	2.19 10^8	1.56	2.66 10^7
Sunlight	3.49 10^7	1.02 10^3	1.67 10^7

Since the conversion only involved the multiplication by constant values (UEVs), the variability of each energy source was not affected and the features showed in the previous paragraph are still valid. On the other hand, the magnitude of the contribution from the emergy perspective was different with respect to the energy one (Fig. 3).

Tides was the global tripartite component that showed the highest maximum and average emergy contribution to the marine system, but they still presented the second lowest minimum. These features show how the contribution of tides is not homogeneous between different marine areas.

The contribution of runoff and rainfall chemical potential was also high. In fact, their high UEV values reflect that they cannot be disregarded when assessing ecological systems (Job and Herrmann, 2006; Lee et al., 2019).

Heat flow and wind emergy resulted to be very close from a maximum and a global average perspective. As stated in Section 3.1, the former heats the deep ocean, thus influencing the large-scale ocean circulation while the latter interacts with the shallower layers driving the surface water movements. Conversely, the wind emergy minimum is still the lowest one among the considered inputs, thus remarking its high global variability.

From a global perspective, we found that all the inputs shared the same order of magnitude (10^7) of the daily average for the 2018 (Fig. 4).

The 2018 total emergy input to the phytoplankton primary production computed from our analysis was 8.26 10^{24} sej y^{-1}

3.3. Global emergy of phytoplankton primary production

Once the global inputs of energy flows were assessed and converted into emergy units, we computed the total emergy supporting phytoplankton primary production (8.26 10^{24} sej y^{-1}) and the emergy to production ratio. The latter allowed to highlight marine system areas that interact differently with the energy inputs. In fact, a large emergy to production ratio was associated to areas which showed either a high level of emergy flows but low phytoplankton production or elevated primary production and huge emergy flows. We analysed the global maps of integrated production, emergy, and emergy to production ratio for 4 different months, which in turn refer to seasonal phases of phytoplankton global cycle (Figs. 5 to 8). From an ecological perspective, we used this analysis to highlight both temporal and spatial patterns associated with phytoplankton production.

January 2018 presented low level of phytoplankton production in most areas of the northern hemisphere (Fig. 5a). This production contraction during the winter months is a common feature at northern temperate latitudes (23.5° to 66.5° N) especially in the north Atlantic, the majority of the north Pacific, and the Mediterranean basins. This phenomenon is mainly due to the lack of solar radiation which plays a key role in the photosynthetic process. This characteristic can be noted also in the emergy map (Fig. 5b), which shows low values for the abovementioned areas. Moreover, the high values of the emergy to production ratio in the rare areas that show high emergy levels highlight the impossibility to convert the available energy into primary production (Fig. 5c). A notable exception to this trend is the high level of production in the Arabian sea since its phytoplankton dynamics are mainly driven by the nutrients upwelling caused by the monsoon cycles that characterize the area (Dickson et al., 2001).

On the other hand, the southern hemisphere shows an opposite trend since solar energy is not a limiting factor during this period of the year. High levels of primary production can be found in the coastal areas of Argentina, Uruguay, and south Brazil. In this continental shelf area, the interactions between Brazil and Malvinas currents generate an upwelling of nutrients, which coupled with favourable irradiation conditions, generates a remarkable magnitude of phytoplankton production. A large share of production characterizes also the southern portion of the oceans, especially along the subtropical front. Favourable conditions for the phytoplankton production are reflected by the emergy to production ratio. In fact, this ratio shows low values in spite of the large level of emergy that characterizes these highly productive areas. This feature suggests that during this period of the year the energy conveyed to the system can be effectively converted into phytoplankton production.

During spring (Fig. 6a) we can notice an enhancement of the primary production in the northern temperate zone. In fact, a spring phytoplankton production peak is a common feature in this area. This peak is fueled by the coupling of a high nutrient concentration in the euphotic zone, which is the result of the low consumption rate during the winter months, and a raise of the irradiance level. Even if we do not have the same spatial coverage of northern hemisphere during January and April, a production enhancement can be shown in the northern part of the Atlantic, Pacific, and Mediterranean basins. We can see this trend in these areas also looking at the emergy to production ratio, which is lower in Fig. 6c with respect to Fig. 5c. Particularly high values of production are found near the coast, where the nutrient inputs from land can deeply influence the phytoplankton growth. This is a general feature of the oceanic production and will be later discussed along with other characteristics that are more dependent on the spatial variability than the temporal one.

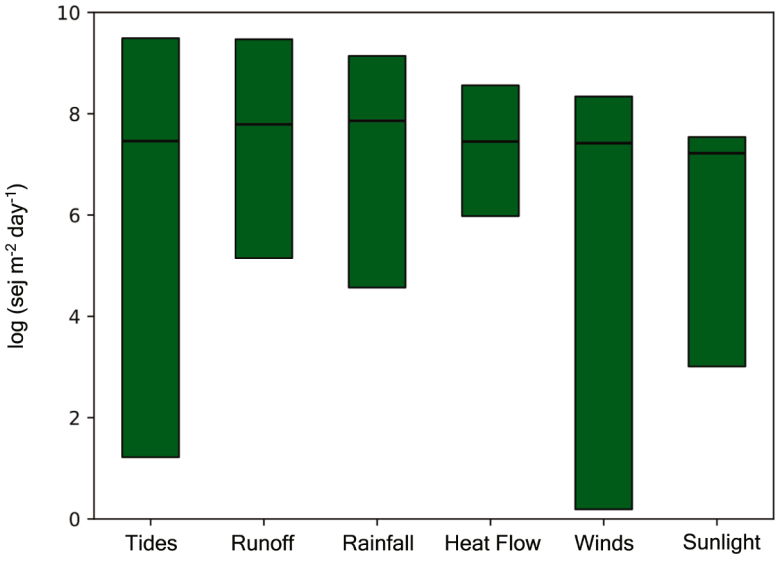

Fig. 4. Daily emergy contribution in 2018. The bar chart shows the emergy daily range and the average emergy value for each input for the year 2018.

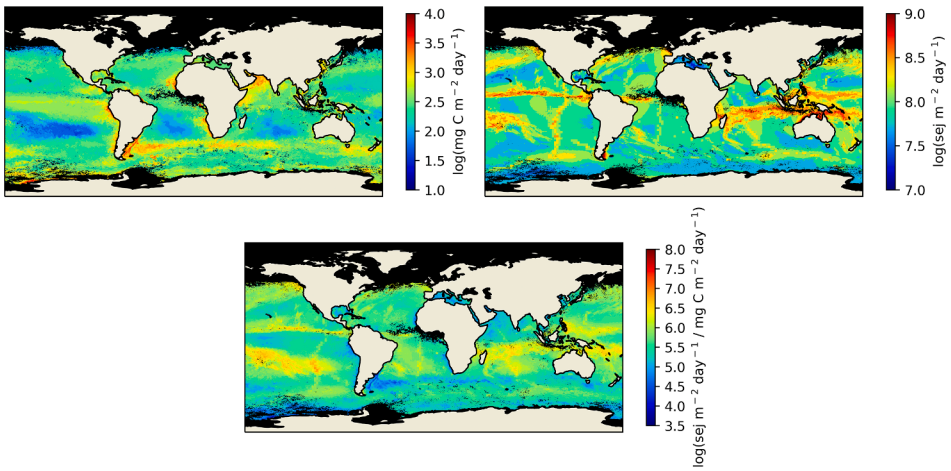

Fig. 5. Global phytoplankton assessment maps. January 2018. a) Integrated primary production, b) Emergy, and c) Emergy to production ratio.

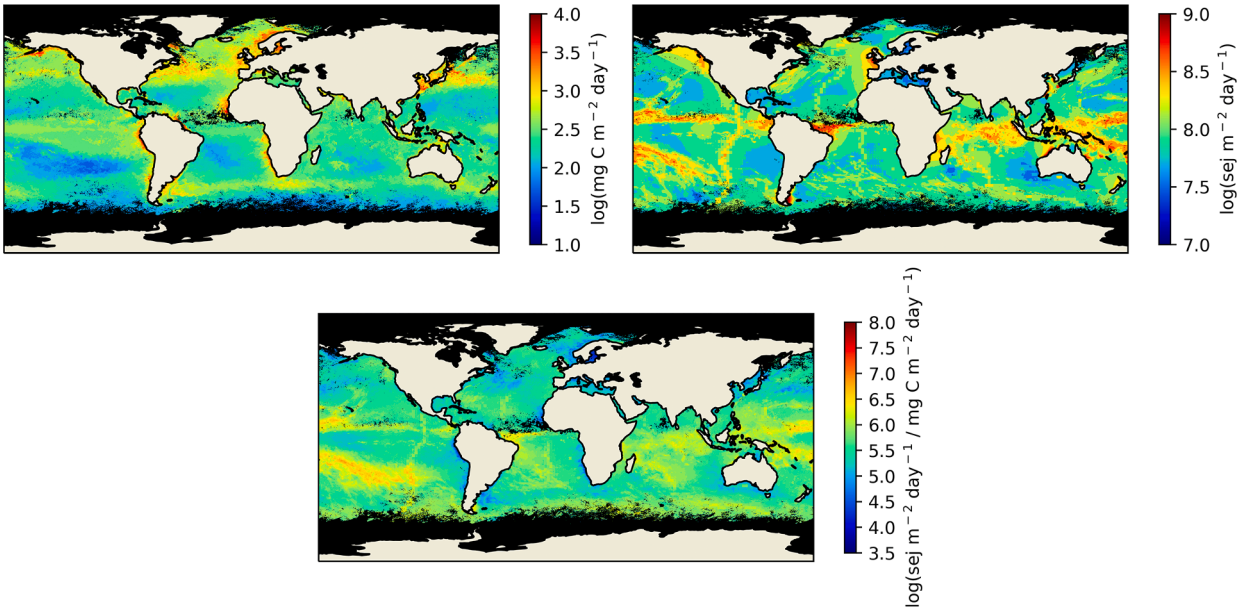

Fig. 6. Global phytoplankton assessment maps. April 2018. a) Integrated primary production, b) Emergy, and c) Emergy to production ratio.

In the southern hemisphere we can observe an overall reduction of primary production with respect to Fig. 5. The decrease is coupled with an increase of the emergy to production ratio, which suggests that external factors such as nutrient depletion and lowering in irradiance could affect primary production.

During the summer months in the northern hemisphere the production peak shifted towards higher latitude. This feature is highlighted by both Fig. 7a and c which showed higher production and lower emergy to production ratio values, respectively. On the other hand, areas in which the nutrients consumed during the spring maximum were not replenished by land inputs showed a decrease in production and a raise in the production to emergy ratio. This is partially due to a strong surface stratification caused by the high level of irradiance that characterizes the summer months. The Mediterranean basin and the strip of the Atlantic Ocean that showed a spring peak fall in the latter described category.

The areas which show a large emergy to production ratio in the higher latitudes are those which also receive a high share of energy. Since phytoplankton production is a biological process it has biological constraints and when the maximum value is reached additional energy will not result in a production enhancement (Fig. 7).

In the southern hemisphere the information was limited since remotely sensed estimates of chlorophyll *a* concentration are not always available. Nonetheless, we can notice a boost in the phytoplankton production coupled with a decrease in the emergy to production ratio along the coast of Africa, Oceania, south America, and south Asia with respect to April (Fig. 6).

The last considered month was October. The overall production magnitude keeps contracting in the north Atlantic and the northeast Pacific Ocean. Conversely, few areas such as the Mediterranean basin and the northwest Pacific experienced a second production peak (Fig. 8a). The former phenomenon was mainly due to the reduction in solar energy during autumn while the latter could be caused by a seasonal mixing that occurs with the lowering of seas surface temperature and the following surface stratification break. This mixing brings nutrients in the euphotic zone thus resulting in a second seasonal peak.

In the southern hemisphere the production raised with respect to April. In fact, in October the irradiance available in this part of the world increases positively influencing the phytoplankton production. Accordingly, the emergy to production ratio was considerably low in the south area of the main basins.

We observed that several patterns highlighted by the emergy

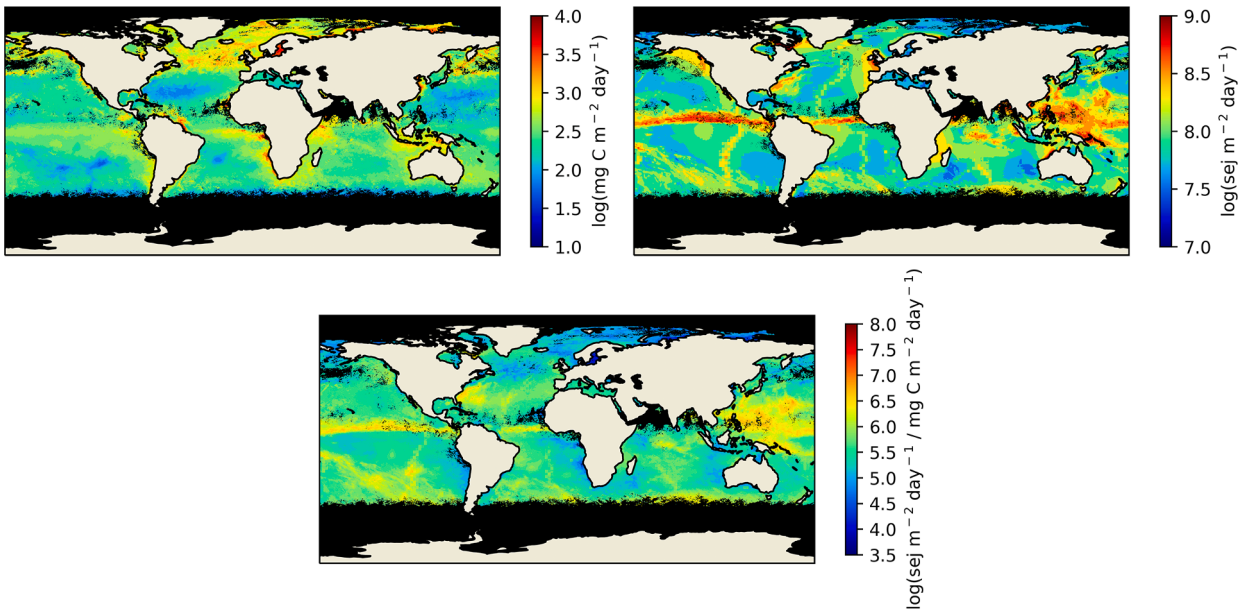

Fig. 7. Global phytoplankton assessment maps. July 2018. a) Integrated primary production, b) Emergy, and c) Emergy to production ratio.

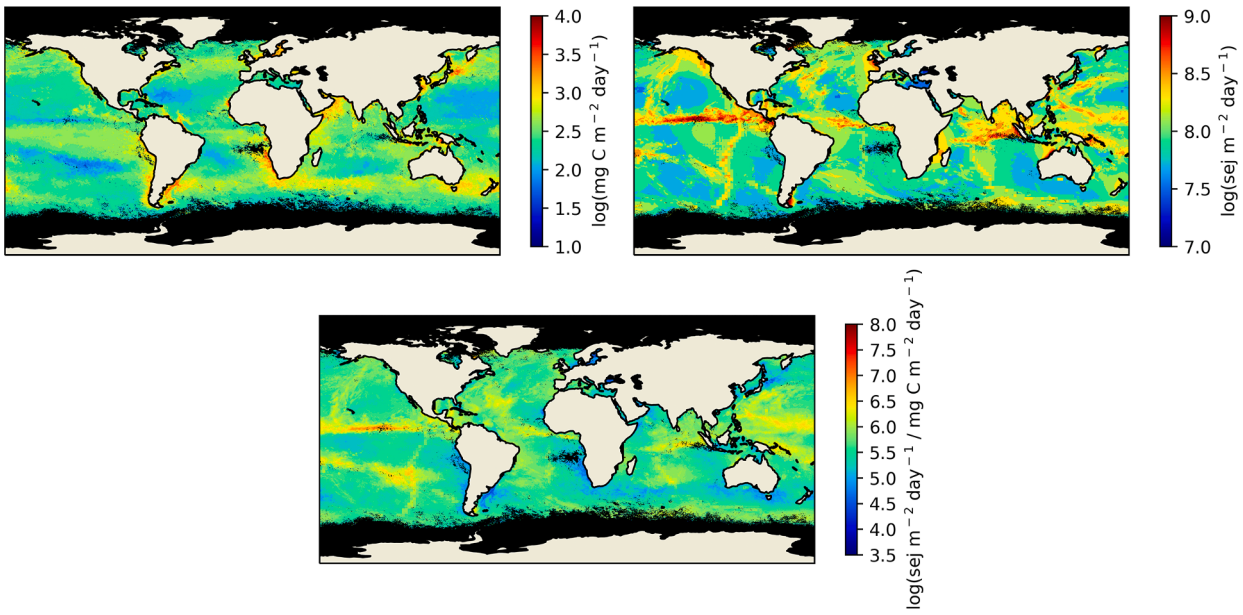

Fig. 8. Global phytoplankton assessment maps. October 2018. a) Integrated primary production, b) Emergy, and c) Emergy to production ratio.

assessment were more dependent on the geographical characteristics of the area than on the seasonal cycle of the phytoplankton production. For instance, the upwelling areas showed common features independently of the season. These areas presented a higher level of production compared to other regions. Moreover, even if the emergy values in these zones were high the emergy to production ratio was consistently low. This feature pointed out how these areas can exploit the energy potential thanks to new nutrients coming from deep layers of the water column. The equatorial Pacific, the coast of Chile, the coast of Peru, the Brazil Malvinas Current interaction zone, the coast of Angola, and the subtropical front perfectly fit this description.

Another general pattern was the tendency to have higher levels of phytoplankton production in coastal areas. In fact, these areas are influenced by nutrient inputs from land or from coastal upwelling phenomena both enhancing primary production.

Conversely, open Ocean regions are often associated with low production values. Sinking of organic matter and water column stratification often lead these areas to nutrient depletion which in turn limits the phytoplankton no matter what energy inputs can fuel the system. For these reasons, open ocean is generally characterized by high level of emergy production ratio.

To further exploit the information provided by the emergy to production ratio, we analysed its variability during the year. Therefore, we computed the variance of this ratio for each pixel that showed less than 6 missing values and less than 3 missing values in a row out of 12, i.e. one for each month. The rationale behind this procedure was to avoid biases in the variance computation due to over- and under- represented periods of the year. The grid obtained was used to produce a map which displays the variability of the emergy to production ratio on a global scale (Fig. 9b).

The exclusion of the areas with not enough data or which presented more than 3 months of missing values in a row led to a loss of

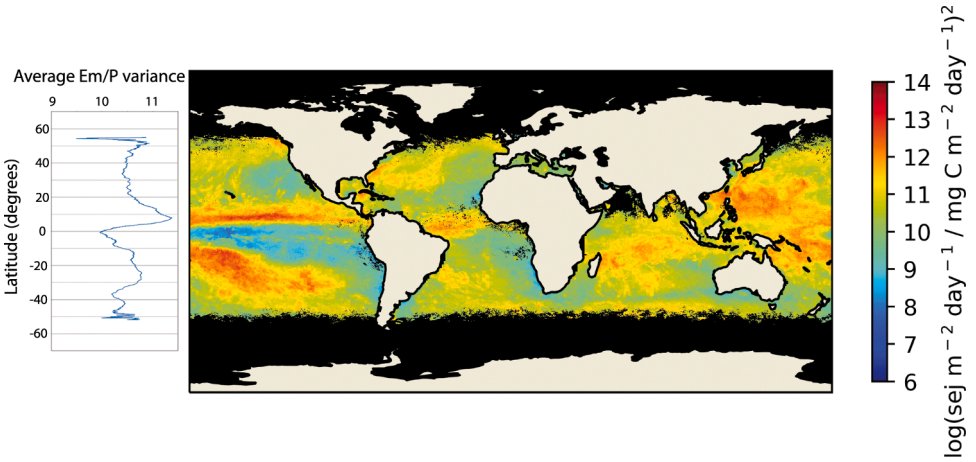

Fig. 9. Variance of the emergy to production ratio during the year 2018. Map of the emergy to production ratio variance (right) and the latitudinal trend of its average (left).

information at higher latitudes. On the other hand, this procedure returned a more reliable variance assessment which in turn led to a more consistent analysis from an ecological perspective. It was not surprising to find a lower variance in the upwelling areas. Since nutrients are the most limiting factor in oceanic phytoplankton production, if an upwelling phenomenon provides continuous fuel for exploiting the potential available energy the production will receive a boost in both magnitude and stability. A stable level of primary production throughout the year is an important feature since it can support the structuring of complex food webs, conveying more energy towards higher trophic levels. In this context, the emergy to primary production ratio can be seen as an inverse measure of energy transfer efficiency in the trophic webs. The equatorial Pacific upwelling system is among the largest and most stable ones. In fact, the Pacific Ocean is one of the most productive fishing grounds in the world, not only due to his large extension but also because it encompasses several upwelling areas. Two of the major upwelling systems in the Atlantic Ocean, i.e. Brazil-Malvinas currents interaction and Angola coast, share the same low variance values.

Not surprisingly, areas subjected to strong seasonality show a larger level of variability. This feature well suits several areas whose characteristics were previously described in this paragraph, such as the north Atlantic and the north and the south Pacific.

The Mediterranean Sea showed a low variance of the emergy to production ratio. This basin is a closed and oligotrophic one, which has an overall low potential in terms of phytoplankton production. Indeed, its low variability of the emergy to production ratio can be interpreted as a consequence of these peculiar features.

Finally, we analysed the latitudinal trend of the emergy to production ratio variance by computing the average of each row in the grid (Fig. 9a). The two hemispheres show different characteristics mainly due to the difference in land coverage, which in turn affects the seasonality and the trends of phytoplankton production.

In the northern hemisphere we saw high levels of variability around 50° N, since this latitude encompasses several areas characterized by strong seasonality. Subsequently, the average values decrease to a local minimum around 40° N. This low variability was due to the presence of the Mediterranean basin, whose low potential heavily affects the average computation in this latitudinal range. The variability remains constant till 32° N where it raised again reaching maximum values around 8° N. This area includes Atlantic and Pacific areas dominated by strong primary production seasonality. From 8° N to the equator the average variability steadily decreased till a minimum value. The low values of variance that characterizes this area could be attributed mainly to the stable environmental conditions of the equator.

In the southern hemisphere the average variability raised to a local maximum value from 0° to roughly 25° S. This area includes coastal and open oceans area with a marked seasonality, e.g. the Indian Ocean. The latter was the first strong difference between the two hemispheres. From 20° to roughly 30° S the average variance oscillates around local maximum values. This feature was due to the presence of both stable areas and areas affected by strong seasonality. In fact, the former latitudes encompass areas such as the Pacific upwelling area, which was one of the most stable and productive, and less stable areas such as the eastern Africa coast and the southern Indian Ocean. Then the average variability dropped till 38° S and showed a second peak around 42° N. Finally, the average emergy to production variance drop again and remains relatively constant till 47° S. This substantial drop was mainly linked to the production stability of the subtropical front which sustains a high level of production throughout the year and was previously highlighted as one of the most productive areas. This was the last evident characteristic that distinguished the two hemispheres. Then the average variability spikes again to maximum values around 52° S where our analysis had to stop due to missing information.

The uncertainties in this work are related to both the primary production and emergy estimates. The former appraisals were produced using an ANN model (Scardi, 2001) which was analysed and compared with several other estimators (Campbell et al., 2002; Carr et al., 2006; Friedrichs et al., 2009; Lee et al., 2015; Saba et al., 2011). The comparison works determined a range of 49–60 Gt C y-1 (Carr et al., 2006) for the global annual phytoplankton production. This uncertainty highlights need to further investigate this important biological process. The high level of variability of this process coupled with data paucity have been recognised as the main limiting factors influencing our ability to model the global marine phytoplankton production. Our analysis of global phytoplankton production is also limited to the ocean areas for which satellite data are available.

From the emergy perspective, the main uncertainties derived from the spatio-temporal coverage of the considered variables and possibility to assess their variability. For example, the tides and the heat flow data used in this work have an annual temporal resolution thus not convoying any inter-annual variability in our analysis. Moreover, the heat flow dataset has a spatial resolution of 1° latitude x 1° longitude. Even on a global scale this coarse resolution limits the spatial details provided by this variable. One possible effect of a coarse input resolution could be the detail loss especially in the land-sea and in the coast-open sea interface. These limitations could be overcome by enhancing the spatio-temporal resolution of the environmental variables used as inputs.

Finally, the access to different estimates for each environmental variable could be useful to assess their uncertainty and how they affect

the global emergy appraisals from a numerical perspective. Unfortunately, it is not an easy task to find global and ready to use datasets for most of the environmental variables used in this work.

4. Conclusions

In this work we combined ML and environmental accounting models to perform a global assessment of phytoplankton primary production. The ANN technique was used to estimate phytoplankton production while the emergy accounting method was used to assess the energy input flows supporting primary production at global scale.

The proposed methodology allowed to analyze both temporal and geographical global patterns of oceanic primary production and to compute an emergy/production ratio showing different global patterns in terms of emergy convergence into the primary production process.

We believe that the assessment of global phytoplankton production proposed in this work could be a valuable tool to enhance our understanding of this pivotal biological process from a systems perspective. The global assessment can also provide a useful benchmark for future assessment of marine ecosystem services at global scale. In fact, phytoplankton production plays a crucial role as energy source for structuring the marine food webs on which, in turn, depends the generation of ecosystem services vital for human well-being. Noteworthy is the potential usefulness of the proposed global assessment for climate change study and modeling considering the tight links that phytoplankton production has with the Earth's climate.

Declaration of Competing Interest

The authors declare that they have no known competing financial interests or personal relationships that could have appeared to influence the work reported in this paper. The authors declare the following financial interests/personal relationships which may be considered as potential competing interests:

Supplementary materials

Supplementary material associated with this article can be found, in the online version, at doi:10.1016/j.ecolmodel.2021.109578.

References

Barange, M., Merino, G., Blanchard, J.L., Scholtens, J., Harle, J., Allison, E.H., Allen, J.I., Holt, J., Jennings, S., 2014. Impacts of climate change on marine ecosystem production in societies dependent on fisheries. Nat. Clim. Change 4, 211–216. https://doi.org/10.1038/nclimate2119.

Beardsmore, G.R., Beardsmore, S.R.F.G.R., Cull, J.P., Cull, James Phillip, 2001. Crustal Heat Flow: A Guide to Measurement and Modelling. Cambridge University Press.

Behrenfeld, M.J., Falkowski, P.G., 1997. Photosynthetic rates derived from satellite-based chlorophyll concentration. Limnol. Oceanogr. 42, 1–20. https://doi.org/10.4319/lo.1997.42.1.0001.

Behrenfeld, M.J., O'Malley, R.T., Siegel, D.A., McClain, C.R., Sarmiento, J.L., Feldman, G.C., Milligan, A.J., Falkowski, P.G., Letelier, R.M., Boss, E.S., 2006. Climate-driven trends in contemporary ocean productivity. Nature 444, 752. https://doi.org/10.1038/nature05317.

Berrios, F., Campbell, D.E., Ortiz, M., 2018. Emergy-based indicators for evaluating ecosystem health: a case study of three benthic ecosystem networks influenced by coastal upwelling in northern Chile (SE Pacific coast). Ecol. Indic. 95, 379–393. https://doi.org/10.1016/j.ecolind.2018.07.055.

Berrios, F., Campbell, D.E., Ortiz, M., 2017. Emergy evaluation of benthic ecosystems influenced by upwelling in northern Chile: contributions of the ecosystems to the regional economy. Ecol. Model. 359, 146–164. https://doi.org/10.1016/j.ecolmodel.2017.05.005.

Blanchard, J.L., Jennings, S., Holmes, R., Harle, J., Merino, G., Allen, J.I., Holt, J., Dulvy, N.K., Barange, M., 2012. Potential consequences of climate change for primary production and fish production in large marine ecosystems. Philos. Trans. R. Soc. B Biol. Sci. 367, 2979–2989. https://doi.org/10.1098/rstb.2012.0231.

Blauw, A.N., Benincà, E., Laane, R.W.P.M., Greenwood, N., Huisman, J., 2012. Dancing with the tides: fluctuations of coastal phytoplankton orchestrated by different oscillatory modes of the tidal cycle. PLoS ONE 7, e49319. https://doi.org/10.1371/journal.pone.0049319.

Blythe, J., Armitage, D., Alonso, G., Campbell, D., Esteves Dias, A.C., Epstein, G., Marschke, M., Nayak, P., 2020. Frontiers in coastal well-being and ecosystem services research: a systematic review. Ocean Coast. Manag. 185, 105028 https://doi.org/10.1016/j.ocecoaman.2019.105028.

Boyce, D.G., Lewis, M.R., Worm, B., 2010. Global phytoplankton decline over the past century. Nature 466, 591–596. https://doi.org/10.1038/nature09268.

Britton, C.M., Dodd, J.D., 1976. Relationships of photosynthetically active radiation and shortwave irradiance. Agric. Meteorol. 17, 1–7. https://doi.org/10.1016/0002-1571(76)90080-7.

Brown, M.T., Campbell, D.E., De Vilbiss, C., Ulgiati, S., 2016. The geobiosphere emergy baseline: a synthesis. Ecol. Model. 339, 92–95. https://doi.org/10.1016/j.ecolmodel.2016.03.018.

Brown, M.T., Ulgiati, S., 2016a. Emergy assessment of global renewable sources. Ecol. Model. 339, 148–156. https://doi.org/10.1016/j.ecolmodel.2016.03.010.

Brown, M.T., Ulgiati, S., 2016b. Assessing the global environmental sources driving the geobiosphere: a revised emergy baseline. Ecol. Model. 339, 126–132. https://doi.org/10.1016/j.ecolmodel.2016.03.017.

Brown, M.T., Ulgiati, S., 2016c. Assessing the global environmental sources driving the geobiosphere: a revised emergy baseline. Ecol. Model. 339, 126–132. https://doi.org/10.1016/j.ecolmodel.2016.03.017.

Buonocore, E., Appolloni, L., Russo, G.F., Franzese, P.P., 2020a. Assessing natural capital value in marine ecosystems through an environmental accounting model: a case study in Southern Italy. Ecol. Model. 419, 108958 https://doi.org/10.1016/j.ecolmodel.2020.108958.

Buonocore, E., Donnarumma, L., Appolloni, L., Miccio, A., Russo, G.F., Franzese, P.P., 2020b. Marine natural capital and ecosystem services: an environmental accounting model. Ecol. Model. 424, 109029 https://doi.org/10.1016/j.ecolmodel.2020.109029.

Buonocore, E., Picone, F., Donnarumma, L., Russo, G.F., Franzese, P.P., 2019. Modeling matter and energy flows in marine ecosystems using emergy and eco-exergy methods to account for natural capital value 392, 137–146. 10.1016/j.ecolmodel.2018.11.018.

Cadier, M., Gorgues, T., LHelguen, S., Sourisseau, M., Memery, L., 2017. Tidal cycle control of biogeochemical and ecological properties of a macrotidal ecosystem. Geophys. Res. Lett. 44, 8453–8462. https://doi.org/10.1002/2017GL074173.

Campbell, J, Antoine, D, Armstrong, R, Arrigo, K, Balch, W, Barber, R, Behrenfeld, M, Bidigare, R, Bishop, J, Carr, M.E, Esaias, W, Falkowski, P, Hoepffner, N, Iverson, R, Kiefer, D, Lohrenz, S, Marra, J, Morel, A, Ryan, J, Vedernikov, V, Waters, K, Yentsch, C, Yoder, J, 2002. Comparison of algorithms for estimating ocean primary production from surface chlorophyll, temperature, and irradiance. Glob. Biogeochem. Cycles 16. https://doi.org/10.1029/2001GB001444.

Campbell, E.T., Tilley, D.R., 2016. Relationships between renewable emergy storage or flow and biodiversity: a modeling investigation. Ecol. Model. 340, 134–148. https://doi.org/10.1016/j.ecolmodel.2016.08.004.

Carr, M.-.E., Friedrichs, M.A.M., Schmeltz, M., Noguchi Aita, M., Antoine, D., Arrigo, K. R., Asanuma, I., Aumont, O., Barber, R., Behrenfeld, M., Bidigare, R., Buitenhuis, E. T., Campbell, J., Ciotti, A., Dierssen, H., Dowell, M., Dunne, J., Esaias, W., Gentili, B., Gregg, W., Groom, S., Hoepffner, N., Ishizaka, J., Kameda, T., Le Quéré, C., Lohrenz, S., Marra, J., Mélin, F., Moore, K., Morel, A., Reddy, T.E., Ryan, J., Scardi, M., Smyth, T., Turpie, K., Tilstone, G., Waters, K., Yamanaka, Y, 2006. A comparison of global estimates of marine primary production from ocean color. Deep Sea Res. Part II Top. Stud. Oceanogr 53, 741–770. https://doi.org/10.1016/j.dsr2.2006.01.028. The US JGOFS Synthesis and Modeling Project: Phase III.

Catucci, E., Scardi, M., 2020. A Machine Learning approach to the assessment of the vulnerability of Posidonia oceanica meadows. Ecol. Indic. 108, 105744 https://doi.org/10.1016/j.ecolind.2019.105744.

Chakraborty, S., Saha, S.K., Ahmed Selim, S., 2020. Recreational services in tourism dominated coastal ecosystems: bringing the non-economic values into focus. J. Outdoor Recreat. Tour. 30, 100279 https://doi.org/10.1016/j.jort.2020.100279.

Chase, Z., Strutton, P.G., Hales, B., 2007. Iron links river runoff and shelf width to phytoplankton biomass along the U.S. West Coast. Geophys. Res. Lett 34. https://doi.org/10.1029/2006GL028069.

Conti, L., Scardi, M., 2010. Fisheries yield and primary productivity in large marine ecosystems. Mar. Ecol. Prog. Ser. 410, 233–244. https://doi.org/10.3354/meps08630.

Costanza, R., d'Arge, R., Groot, R.de, Farber, S., Grasso, M., Hannon, B., Limburg, K., Naeem, S., O'Neill, R.V., Paruelo, J., Raskin, R.G., Sutton, P., Belt van den, M., 1997. The value of the world's ecosystem services and natural capital. Nature 387, 253. https://doi.org/10.1038/387253a0.

Davies, J.H., 2013. Global map of solid Earth surface heat flow. Geochem. Geophys. Geosystems 14, 4608–4622. https://doi.org/10.1002/ggge.20271.

Dickson, M.-.L., Orchardo, J., Barber, R., Marra, J., Mccarthy, J., Sambrotto, R., 2001. Production and respiration rates in the Arabian Sea during the 1995 Northeast and Southwest Monsoons. Deep Sea Res. Part II Top. Stud. Oceanogr. 48, 1199–1230. https://doi.org/10.1016/S0967-0645(00)00136-3.

Doney, S.C., 1995. Irreversible thermodynamics and air-sea exchange. J. Geophys. Res. Oceans 100, 8541–8553. https://doi.org/10.1029/95JC00685.

Duarte, C.M., Cebrián, J., 1996. The fate of marine autotrophic production. Limnol. Oceanogr. 41, 1758–1766. https://doi.org/10.4319/lo.1996.41.8.1758.

Fahnestock, M., Abdalati, W., Joughin, I., Brozena, J., Gogineni, P., 2001. High geothermal heat flow, basal melt, and the origin of rapid ice flow in central greenland. Science 294, 2338–2342. https://doi.org/10.1126/science.1065370.

Franceschini, S., Mattei, F., D'Andrea, L., Di Nardi, A., Fiorentino, F., Garofalo, G., Scardi, M., Cataudella, S., Russo, T., 2019. Rummaging through the bin: modelling marine litter distribution using Artificial Neural Networks. Mar. Pollut. Bull. 149, 110580 https://doi.org/10.1016/j.marpolbul.2019.110580.

Franzese, P.P., Brown, M.T., Ulgiati, S., 2014. Environmental accounting: emergy, systems ecology, and ecological modelling. Ecol. Model. Complete 1–3. https://doi.org/10.1016/j.ecolmodel.2013.10.007.
Franzese, P.P., Buonocore, E., Donnarumma, L., Russo, G.F., 2017. Natural capital accounting in marine protected areas: the case of the Islands of Ventotene and S. Stefano (Central Italy). Ecol. Model. 360, 290–299. https://doi.org/10.1016/j.ecolmodel.2017.07.015.
Franzese, P.P., Liu, G., Aricò, S., 2019. Environmental accounting models and nature conservation strategies. Ecol. Model. 397, 36–38. https://doi.org/10.1016/j.ecolmodel.2019.01.015.
Franzese, P.P., Manes, F., Scardi, M., Riccio, A., 2020. Modelling matter and energy flows in the biosphere and human economy. Ecol. Model. 422, 108984 https://doi.org/10.1016/j.ecolmodel.2020.108984.
Franzese, P.P., Rydberg, T., Russo, G.F., Ulgiati, S., 2009. Sustainable biomass production: a comparison between Gross Energy Requirement and Emergy Synthesis methods. Ecol. Indic. 9, 959–970. https://doi.org/10.1016/j.ecolind.2008.11.004.
Friedrichs, M.A.M., Carr, M.-.E., Barber, R.T., Scardi, M., Antoine, D., Armstrong, R.A., Asanuma, I., Behrenfeld, M.J., Buitenhuis, E.T., Chai, F., Christian, J.R., Ciotti, A.M., Doney, S.C., Dowell, M., Dunne, J., Gentili, B., Gregg, W., Hoepffner, N., Ishizaka, J., Kameda, T., Lima, I., Marra, J., Mélin, F., Moore, J.K., Morel, A., O'Malley, R.T., O'Reilly, J., Saba, V.S., Schmeltz, M., Smyth, T.J., Tjiputra, J., Waters, K., Westberry, T.K., Winguth, A., 2009. Assessing the uncertainties of model estimates of primary productivity in the tropical Pacific Ocean. J. Mar. Syst. 76, 113–133. https://doi.org/10.1016/j.jmarsys.2008.05.010. Skill assessment for coupled biological/physical models of marine systems.
Frouin, R., McPherson, J., Ueyoshi, K., Franz, B.A., 2012. A time series of photosynthetically available radiation at the ocean surface from SeaWiFS and MODIS data, in: remote Sensing of the Marine Environment II. Presented at the Remote Sensing of the Marine Environment II. International Society for Optics and Photonics, 852519. https://doi.org/10.1117/12.981264.
Frouin, R., Pinker, R.T., 1995. Estimating Photosynthetically Active Radiation (PAR) at the earth's surface from satellite observations. Remote Sens. Environ., Remote Sensing of Land Surface for Studies of Global Chage 51, 98–107. 10.1016/0034-4257(94)00068-X.
Garratt, J.R., 1994. Review: the atmospheric boundary layer. Earth-Sci. Rev. 37, 89–134. https://doi.org/10.1016/0012-8252(94)90026-4.
Hersbach, H., Bell, W., Berrisford, P., Horányi, A., J., M.-.S., Nicolas, J., Radu, R., Schepers, D., Simmons, A., Soci, C., Dee, D., Dee, D., 2019. Global reanalysis: goodbye ERA-Interim, hello ERA5.
Hu, C., Lee, Z., Franz, B., 2012. Chlorophyll aalgorithms for oligotrophic oceans: a novel approach based on three-band reflectance difference. J. Geophys. Res. Oceans 117. https://doi.org/10.1029/2011JC007395.
Job, G., Herrmann, F., 2006. Chemical potential—A quantity in search of recognition. Eur. J. Phys. 27, 353–371. https://doi.org/10.1088/0143-0807/27/2/018.
Jorge, V.N., Beusekom, J.E.E.van, 1995. Wind- and tide-induced resuspension of sediment and microphytobenthos from tidal flats in the Ems estuary. Limnol. Oceanogr. 40, 776–778. https://doi.org/10.4319/lo.1995.40.4.0776.
Jørgensen, S.E., Fath, B.D., 2004. Application of thermodynamic principles in ecology. Ecol. Complex. 1, 267–280. https://doi.org/10.1016/j.ecocom.2004.07.001.
Jørgensen, S.E., Fath, B.D., Bastianoni, S., Marques, J.C., Muller, F., Nielsen, S.N., Patten, B.D., Tiezzi, E., Ulanowicz, R.E., 2011. A New Ecology: Systems Perspective. Elsevier.
Jørgensen, S.E., Mejer, H., 1979. A holistic approach to ecological modelling. Ecol. Model. 7, 169–189. https://doi.org/10.1016/0304-3800(79)90068-1.
Lee, D., Brown, M., Liu, G., 2019. Renewable Empower Distribution of the World. https://doi.org/10.5890/JEAM.2019.03.003.
Lee, Y.J., Matrai, P.A., Friedrichs, M.A.M., Saba, V.S., Antoine, D., Ardyna, M., Asanuma, I., Babin, M., Bélanger, S., Benoît-Gagné, M., Devred, E., Fernández-Méndez, M., Gentili, B., Hirawake, T., Kang, S.-.H., Kameda, T., Katlein, C., Lee, S.H., Lee, Z., Mélin, F., Scardi, M., Smyth, T.J., Tang, S., Turpie, K.R., Waters, K.J., Westberry, T.K., 2015. An assessment of phytoplankton primary productivity in the Arctic Ocean from satellite ocean color/in situ chlorophyll-a based models. J. Geophys. Res. Oceans 120, 6508–6541. https://doi.org/10.1002/2015JC011018.
Lek, S., Delacoste, M., Baran, P., Dimopoulos, I., Lauga, J., Aulagnier, S., 1996. Application of neural networks to modelling nonlinear relationships in ecology. Ecol. Model. 90, 39–52. https://doi.org/10.1016/0304-3800(95)00142-5.
Levitus, S., Boyer, T.P., 1994. World Ocean Atlas 1994. Volume 4. Temperature (No. PB-95-270112/XAB; NESDIS-4). National Environmental Satellite, Data, and Information Service, Washington, DC (United States).
Levitus, S., Burgett, R., Boyer, T.P., 1994. World Ocean Atlas 1994. Volume 3. Salinity (No. PB-95-270104/XAB; NESDIS-3). National Environmental Satellite, Data, and Information Service, Washington, DCUnited States.
Longhurst, A.R., Glen Harrison, W., 1989. The biological pump: profiles of plankton production and consumption in the upper ocean. Prog. Oceanogr. 22, 47–123. https://doi.org/10.1016/0079-6611(89)90010-4.
Manwell, J.F., McGowan, J.G., Rogers, A.L., 2010. Wind Energy Explained: Theory, Design and Application. John Wiley & Sons.
Mashayek, A., Ferrari, R., Vettoretti, G., Peltier, W.R., 2013. The role of the geothermal heat flux in driving the abyssal ocean circulation: geothermal heat flux and ocean circulation. Geophys. Res. Lett. 40, 3144–3149. https://doi.org/10.1002/grl.50640.
Mattei, F., Franceschini, S., Scardi, M., 2018. A depth-resolved artificial neural network model of marine phytoplankton primary production. Ecol. Model. 382, 51–62. https://doi.org/10.1016/j.ecolmodel.2018.05.003.
Mattei, F., Scardi, M., 2020. Embedding ecological knowledge into artificial neural network training: a marine phytoplankton primary production model case study. Ecol. Model. 421, 108985 https://doi.org/10.1016/j.ecolmodel.2020.108985.
Maureaud, A., Gascuel, D., Colléter, M., Palomares, M.L.D., Du Pontavice, H., Pauly, D., Cheung, W.W.L., 2017. Global change in the trophic functioning of marine food webs. PLoS ONE 12, e0182826. https://doi.org/10.1371/journal.pone.0182826.
Melaku Canu, D., Ghermandi, A., Nunes, P.A.L.D., Lazzari, P., Cossarini, G., Solidoro, C., 2015. Estimating the value of carbon sequestration ecosystem services in the Mediterranean Sea: an ecological economics approach. Glob. Environ. Change 32, 87–95. https://doi.org/10.1016/j.gloenvcha.2015.02.008.
Morel, A., Maritorena, S., 2001. Bio-optical properties of oceanic waters: a reappraisal. J. Geophys. Res. Oceans 106, 7163–7180. https://doi.org/10.1029/2000JC000319.
Nixon, S.W., 1992. Quantifying the relationship between nitrogen input and the productivity of marine ecosystem. Adv Mar Tech Conf Tokyo 5, 57–83.
Odum, H.T., 1996. Environmental accounting: Emergy and Environmental Decision Making. Wiley, Chichester.
Odum, H.T., 1988. Self-Organization, Transformity, and Information. Science 242, 1132–1139. https://doi.org/10.1126/science.242.4882.1132.
Olden, J.D., Lawler, J.J., Poff, N.L., 2008. Machine learning methods without tears: a primer for ecologists. Q. Rev. Biol. 83, 171–193. https://doi.org/10.1086/587826.
O'Reilly, J.E., Maritorena, S., Mitchell, B.G., Siegel, D.A., Carder, K.L., Garver, S.A., Kahru, M., McClain, C., 1998. Ocean color chlorophyll algorithms for SeaWiFS. J. Geophys. Res. Oceans 103, 24937–24953. https://doi.org/10.1029/98JC02160.
Paoli, C., Povero, P., Burgos, E., Dapueto, G., Fanciulli, G., Massa, F., Scarpellini, P., Vassallo, P., 2018. Natural capital and environmental flows assessment in marine protected areas: the case study of Liguria region (NW Mediterranean Sea). Ecol. Model 368, 121–135. https://doi.org/10.1016/j.ecolmodel.2017.10.014.
Picone, F., Buonocore, E., D'Agostaro, R., Donati, S., Chemello, R., Franzese, P.P., 2017. Integrating natural capital assessment and marine spatial planning: a case study in the Mediterranean sea. Ecol. Model. 361, 1–13. https://doi.org/10.1016/j.ecolmodel.2017.07.029.
Pulselli, F.M., Coscieme, L., Bastianoni, S., 2011. Ecosystem services as a counterpart of emergy flows to ecosystems. Ecol. Model., Non-equilibrium Thermodynamics in Ecology 222, 2924–2928. https://doi.org/10.1016/j.ecolmodel.2011.04.022.
Reynolds, C.S., 2006. The Ecology of Phytoplankton. Cambridge University Press.
Richardson, A.J., Schoeman, D.S., 2004. Climate impact on plankton ecosystems in the Northeast Atlantic. Science 305, 1609–1612. https://doi.org/10.1126/science.1100958.
Rumelhart, D.E., Hinton, G.E., Williams, R.J., 1986. Learning representations by back-propagating errors. Nature 323, 533. https://doi.org/10.1038/323533a0.
Russo, T., Carpentieri, P., D'Andrea, L., De Angelis, P., Fiorentino, F., Franceschini, S., Garofalo, G., Labanchi, L., Parisi, A., Scardi, M., Cataudella, S., 2019. Trends in effort and yield of trawl fisheries: a case study from the Mediterranean Sea. Front. Mar. Sci. 6 https://doi.org/10.3389/fmars.2019.00153.
Saba, V.S., Friedrichs, M.a.M., Antoine, D., Armstrong, R.A., Asanuma, I., Behrenfeld, M. J., Ciotti, A.M., Dowell, M., Hoepffner, N., Hyde, K.J.W., Ishizaka, J., Kameda, T., Marra, J., Mélin, F., Morel, A., O'Reilly, J., Scardi, M., Smith Jr., W.O., Smyth, T.J., Tang, S., Uitz, J., Waters, K., Westberry, T.K., 2011. An evaluation of ocean color model estimates of marine primary productivity in coastal and pelagic regions across the globe. Biogeosciences 8, 489–503. https://doi.org/10.5194/bg-8-489-2011.
Scardi, M., 2001. Advances in neural network modeling of phytoplankton primary production. Ecol. Model. 146, 33–45. https://doi.org/10.1016/S0304-3800(01)00294-0.
Schlössel, P., Soloviev, A.V., Emery, W.J., 1997. Cool and freshwater skin of the ocean during rainfall. Bound.-Layer Meteorol. 82, 439–474. 10.1023/A:1000225700380.
Scott, J.R., Marotzke, J., Adcroft, A., 2001. Geothermal heating and its influence on the meridional overturning circulation. J. Geophys. Res. Oceans 106, 31141–31154. https://doi.org/10.1029/2000JC000532.
Spatharis, S., Mouillot, D., Danielidis, D.B., Karydis, M., Chi, T.D., Tsirtsis, G., 2008. Influence of terrestrial runoff on phytoplankton species richness-biomass relationships: a double stress hypothesis. J. Exp. Mar. Biol. Ecol. 362, 55–62. https://doi.org/10.1016/j.jembe.2008.06.003.
Vassallo, P., Paoli, C., Buonocore, E., Franzese, P.P., Russo, G.F., Povero, P., 2017. Assessing the value of natural capital in marine protected areas: a biophysical and trophodynamic environmental accounting model. Ecol. Model. 355, 12–17. https://doi.org/10.1016/j.ecolmodel.2017.03.013.
Vihervaara, P, Franzese, P.P, Buonocore, E, 2019. Information, energy, and eco-exergy as indicators of ecosystem complexity. Ecological Modelling 395, 23–27. https://doi.org/10.1016/j.ecolmodel.2019.01.010.
Werdell, P.J., Bailey, S.W., 2005. An improved in-situ bio-optical data set for ocean color algorithm development and satellite data product validation. Remote Sens. Environ. 98, 122–140. https://doi.org/10.1016/j.rse.2005.07.001.
Werdell, P.J., Franz, B.A., Bailey, S.W., Feldman, G.C., Boss, E., Brando, V.E., Dowell, M., Hirata, T., Lavender, S.J., Lee, Z., Loisel, H., Maritorena, S., Mélin, F., Moore, T.S., Smyth, T.J., Antoine, D., Devred, E., d'Andon, O.H.F., Mangin, A., 2013. Generalized ocean color inversion model for retrieving marine inherent optical properties. Appl. Opt. 52, 2019–2037. https://doi.org/10.1364/AO.52.002019.
Yang, Q., Liu, G., Casazza, M., Hao, Y., Giannetti, B.F., 2019. Emergy-based accounting method for aquatic ecosystem services valuation: a case of China. J. Clean. Prod. 230, 55–68. https://doi.org/10.1016/j.jclepro.2019.05.080.
Zhai, X., 2013. On the wind mechanical forcing of the ocean general circulation. J. Geophys. Res. Oceans 118, 6561–6577. https://doi.org/10.1002/2013JC009086.